ChemPubSoc Europe

DOI: 10.1002/chem.201903631

CHEMISTRY A European Journal Full Paper

Nanostructures | *Hot Paper*

Turning DNA Binding Motifs into a Material for Flow Cells

Tobias Feldner, Manpreet Wolfrum, and Clemens Richert*[a]

Abstract: Nanoscale assemblies of DNA strands are readily designed and can be generated in a wide range of shapes and sizes. Turning them into solids that bind biomolecules reversibly, so that they can act as active material in flow cells, is a challenge. Among the biomolecular ligands, cofactors are of particular interest because they are often the most expensive reagents of biochemical transformations, for which controlled release and recycling are desirable. We have recently described DNA triplex motifs that bind adenine-containing cofactors, such as NAD, FAD and ATP, reversibly with low micromolar affinity. We sought ways to convert the soluble DNA motifs into a macroporous solid for cofactor binding. While assemblies of linear and branched DNA motifs produced hydrogels with undesirable properties, long DNA triplexes treated with protamine gave materials suitable for flow cells. Using exchangeable cells in a flow system, thermally controlled loading and discharge were demonstrated. Employing a flow cell loaded with ATP, bioluminescence was induced through thermal release of the cofactor. The results show that materials generated from functional DNA structures can be successfully employed in macroscopic devices.

Introduction

One of the most successful ways to develop macromolecular objects from biodegradable starting materials is DNA nanostructuring.[1–3] Using designs based on double helices and assembling by base pairing between complementary stretches of sequence, nanoscale structures can be produced.[4,5] A broad range of sizes,[6] as well as intricate shapes,[7] have been constructed in this fashion. Applications in drug delivery[8] have been proposed and spatially controlled chemical reactions have been demonstrated,[9] but turning such aesthetically pleasing three-dimensional DNA nanostructures into functional materials has proven far from trivial.

New functional materials are sought in the field of renewable energy to reduce the environmental impacts caused by traditional technologies. In some instances, nature can be an inspiration for new technologies. Nature produces energy-rich molecules via sustainable processes and stores them, for example, in the form of carbohydrates accumulated in amyloplasts in the underground storage tissues of potato tubers.[10] The biosynthesis and metabolic degradation of carbohydrate polymers requires complex biochemical machineries, though, and this form of chemical build-up and storage of biopolymers is for long-term storage, on the time scale of seasons. Other biological energy storage polymers, such as glycogen, are consumed more quickly in the body, but still require elaborate biochemical machineries. For novel applications in biotechnology or bioenergy, it is easier to employ molecules nature uses for short-term energy storage. Among the best known examples are adenosine triphosphate (ATP), which is frequently utilized in artificial single-enzyme systems,[11] and reduced redox cofactors that feed into the respiratory chain, such as NADH and $FADH_2$.[12] These cofactors are valuable starting materials for biotransformations and recycling them is desirable for efficient processes.[13]

It was unclear whether DNA structures can play a role in capturing cofactors. Nature evolved DNA and RNA to serve as genetic material, not as storage material. Some polynucleotide sequences can fold into binding motifs, however, and ATP was one of the first molecules that were successful bound by RNA sequences evolved in vitro.[14] But, DNA and RNA are polyanions that are well soluble in water. They do not form materials with a structure mimicking that of typical biological storage materials. If DNA is to be condensed, nature usually packages it in the form or chromatin, with nucleosomes as subunits.[15] Nucleosomes contain many costly proteins and too little DNA to make them an attractive component of designed functional materials for storing energy-rich biomolecules. Simpler assemblies are required for practical applications.

We have recently described designed binding motifs made up of DNA or RNA triplexes with gaps that serve as binding sites for purine-containing ligands.[16] Other groups have used modified triplexes with gaps as sensors for purine ligands.[17] The positioning of the binding sites and linkers for bridging the gaps,[18] as well as the number of gaps in longer triplexes[19]

[a] *T. Feldner, M. Wolfrum, Prof. C. Richert*
Institut für Organische Chemie, Universität Stuttgart
Pfaffenwaldring 55, 70569 Stuttgart (Germany)
E-mail: lehrstuhl-2@oc.uni-stuttgart.de

Supporting information and the ORCID identification number(s) for the author(s) of this article can be found under: https://doi.org/10.1002/chem.201903631.

have been optimized. Triplex motifs made up of RNA and encoded in DNA have also been expressed in live cells, resulting in the capture of the second messenger cGMP in vivo.[20] This was encouraging, but did not provide a solution to the challenge of constructing a flow cell visualized in Figure 1. A method had to be developed to turn soluble DNA motifs with binding sites for purine cofactors into a material suitable for flow cells acting as "biochemical batteries".

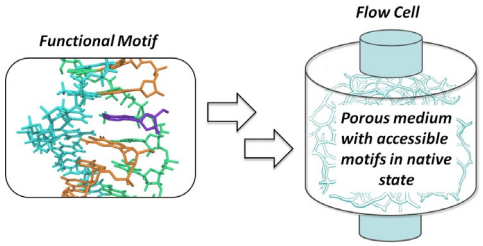

Figure 1. Cartoon visualizing the challenge of turning a functional, soluble DNA motif into a porous material as active matrix of a flow cell.

To achieve this, the method had to be non-denaturing. Further, it had to produce a material suitable for bulk flow through a cartridge. The active material had to bind FAD or ATP at low temperature and release either cofactor upon demand, for example, upon warming to body temperature. In our earlier work, we had immobilized triplex binding motifs on sepharose to obtain a biomaterial that binds cofactors reversibly.[21] The disadvantage of this approach was the low storage capacity, as the sepharose makes up well over 90% of the dry weight of the overall material, with a small fraction remaining for the active DNA motifs. The loading capacity of the new material was to be much higher than that of the sepharose-based one. To achieve this, we focused on molecular assemblies in which DNA serves both as the binding motif and as the (or one) scaffold material. The material had to be porous enough to allow for rapid flow to avoid being limited to slow, diffusion-based processes. We assumed that solutions to this challenge would also pave the way for turning other nanoscale DNA structures into functional materials. Here we report the results of a screen of DNA motifs and a first prototype of a flow cell that captures and releases cofactors.

Results and Discussion

Since DNA motifs can be induced to assemble into crystalline lattices,[22,23] we initially focused on DNA motifs with sticky ends and hybridization-based assembly processes.[24–27] Figure 2 shows the designs tested to obtain cofactor-binding materials. Either of the DNA motifs contains triplex regions with one or several binding sites for purine-containing cofactors. The gaps acting as binding sites were designed to bind adenosine derivatives through a combination of Watson–Crick and Hoogsteen base pairing.[16,19] In the binding sites of the triplexes, the adenine rings also experience stacking interactions on both sides of the π-system, leading to high affinity binding.

Four designs were studied. The first one employed two different "Y-motif" structures with binding sites bridged by $(dC)_6$ linkers and with sticky ends that are complementary to each

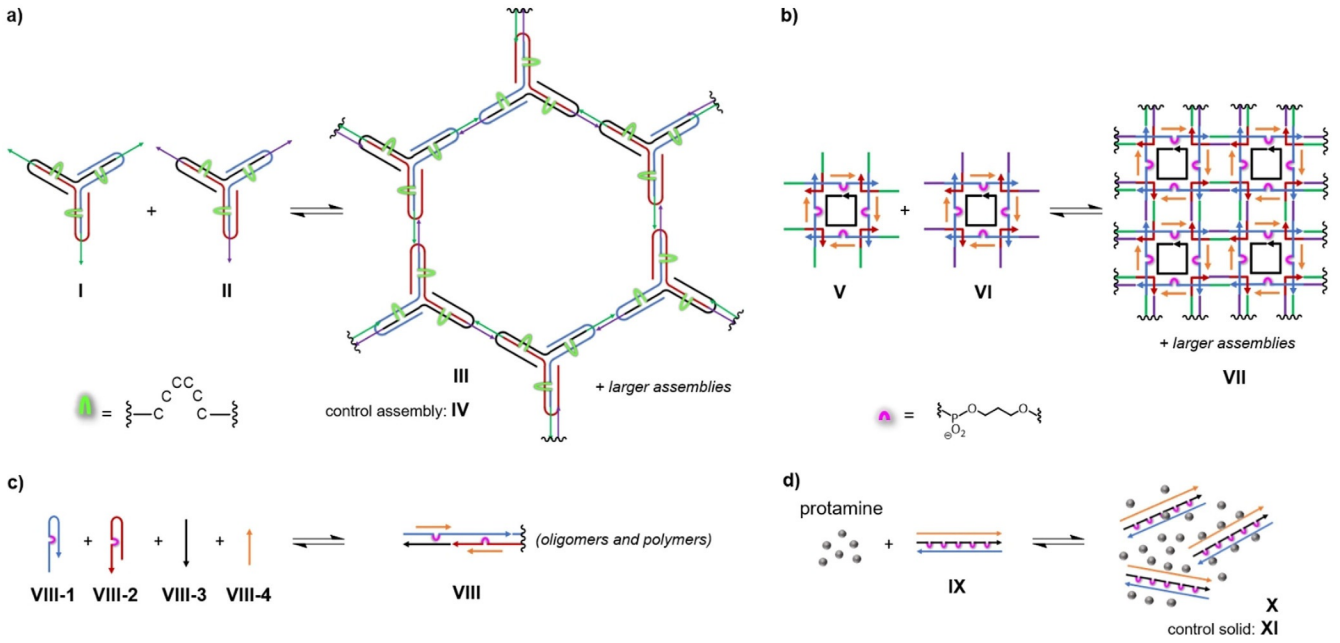

Figure 2. Designed binding motifs tested and multimolecular assemblies formed from them. Controls were assembled from motifs that lack binding sites and feature a continuous oligopurine segment with dA residues instead of bridged gaps. a) Y-Motifs **I** and **II** and the honeycomb assemblies **III**/**IV** formed from them through hybridization of sticky ends. b) Square motifs **V**/**VI** and the assembly produced from them (**VII**). c) Hybridization polymer **VIII** generated from strands **VIII-1**–**4** through hybridization chain reaction. d) Linear triplex motif **IX** precipitated as solid **X** upon addition of protamine and the binding-site free control material **XI**. See the Supporting Information for full sequences and details.

other (**I** and **II**, Figure 2a). Other Y-motifs have been described in the past,[28] and so have triplex-containing nanoscale DNA objects.[29] Base pairing between the sticky ends was expected to produce networks of type **III** with a honeycomb-like arrangement. Besides the assembly with binding sites, control structures without gaps (**IV**) were prepared as negative controls for binding assays.

The second type of assemblies studied were based on "square motifs" **V** and **VI** (Figure 2b). The designs were loosely based on smaller, duplex-based squares combined with segments from triplex-containing triangles published by Seeman and colleagues.[29,30] The triplex-forming oligonucleotide in our designs was 13 nucleotides long, and the gap in the central oligopurine strand of the triplexes was bridged by propylene-phosphate linkers,[17–19,31] indicated as purple arches in Figure 2. Assembly **VII** was to be formed by hybridization of decamer sticky ends. Exploratory work with square motifs containing three bridged gaps gave unsatisfactory results in assembly studies and were not pursued further.

The third design tested was based on linear hybridization polymers (Figure 2c), to be produced by what is known as "hybridization chain reaction".[32] Two metastable hairpins (**VIII-1**/**VIII-2**) containing the bridged nicks, designed to set up binding sites in the final polymer (**VIII**), were used to form long duplexes. Hybridization was triggered by initiator strand **VIII-3**, leading to the chain reaction that corresponds to "polymerization" in covalent chemistry. Average molecular weights of the HCR product are known to depend inversely on the initiator concentration.[32] The triplex-forming octadecamer **VIII-4** was then hybridized to the duplexes to form triplex regions with binding sites for adenine-containing cofactors.

The final design employed in our study used a linear triplex (**IX**), made up of three 45 residue strands with five propylene phosphate-bridged gaps in the central oligopurine. This construct does not feature sticky ends. Instead, precipitation with salmon protamine,[33] arginine-rich cationic peptides known to bind electrostatically to the backbone of DNA, was to be used as the material-forming step (Figure 2d). Besides material **X**, the control material **XI** was assembled, using a continuous oligopurine strand without gaps. Chapter 2 in the Supporting Information gives details of the designs and the full sequences of all strands employed in our study.

Folding of motifs **I**, **II**, **V**, and **VI** was induced by annealing with a linear temperature gradient from 85 °C to 4 °C over 3 d in phosphate buffer containing 150 mM NaCl and 10 mM $MgCl_2$. For motif **IX**, annealing was performed using a water bath that was allowed to cool from 85 °C to 22 °C, followed by cooling to 4 °C for 3 h. Gel electrophoresis confirmed successful folding of the nanostructures. Motifs **I** and **II** showed sharp bands at approx. 300 base pairs (bp), and motifs **V** and **VI** migrated at approx. 250 bp, as calibrated with linear duplexes (Figures 3a and b). The formation of triplex **IX** was confirmed by UV-melting curve analysis (Figure S7, Supporting Information), not gels. The curve was sigmoidal with a shoulder for the triplex-to-duplex transition, giving T_m values of 49.5 °C (triplex) and 59.5 °C (duplex).

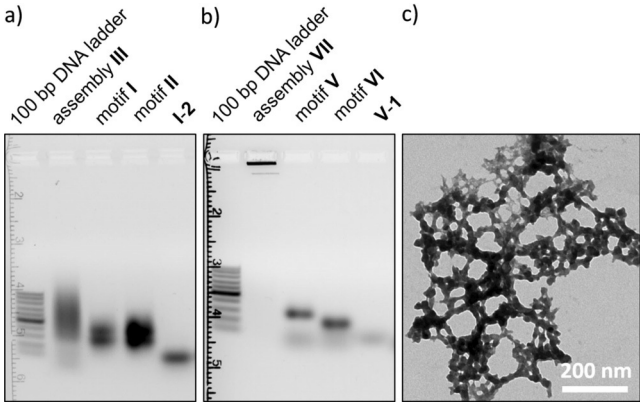

Figure 3. Characterization of DNA assemblies. a) Native agarose electrophoresis gel of assembly **III**, as well as motifs **I** and **II**. Lanes: 1. 100 bp DNA ladder, 2. assembly **III**, 3. motif **I**, 4. motif **II**, 5. oligonucleotide **I-2**. Conditions: 1% agarose gel, Tris/Acetic Acid/EDTA (TAE) buffer, pH 6, 60 V, 4 °C, 2.5 h, staining with GelRed. b) Native agarose gel of square motifs **V** and **VI** and assembly **VII** formed from them. Lanes: 1. 100 bp DNA ladder, 2. assembly **VII**, 3. motif **V**, 4. motif **VI**, 5. oligonucleotide **V-1**. Conditions: 1% agarose gel, TAE buffer, pH 6, 5 mM $MgCl_2$, 2 h, 60 V, 4 °C; staining with GelRed. c) Transmission electron microscopy (TEM) image of **VII**, after staining with uranyl formate. Magnification as indicated by the scale bar.

Next, the ability of the individual motifs to bind purine-containing ligands was determined in equilibrium filtration assays.[16] For the multimolecular assemblies with several binding sites, apparent dissociation constants ($K_{d,app}$) were determined, meaning that binding sites were treated as independent of each other. The results are shown in Table 1. It can be discerned that all designed motifs bind FAD with K_d values in the micromolar range. The lowest dissociation constant was for motif **I**, at 9 μM. Motif **IX** with five binding sites gave apparent dissociation constants of 15 μM for FAD and 36 μM for ATP. The higher value for ATP is expected because FAD can bind through a combination of base pairing and intercalation, and the triphosphate moiety of ATP induces more significant electrostatic repulsion than the pyrophosphate linker of FAD.

The assembly into higher order structures was studied next. Equimolar amounts of motifs with complementary overhangs were mixed to give a final concentration of 4 μM motifs, and the solution was cooled to 4 °C for 12 h, followed by analysis

Table 1. Apparent dissociation constants of complexes of triplex motif-containing assemblies and FAD or ATP.[a]

Triplex motif	binding sites	ligand	$K_{d,app}$[b] [μM] per motif
I	3	FAD	9
V	4	FAD	46
VIII	2	FAD	9
IX	5	FAD	15
IX	5	ATP	36

[a] Conditions: 10 μM motif for **I**, 7.5 μM motif for **V**, 20 μM motif for **VIII**, and 14 μM motif for **IX**; one equiv of ligand per binding site, 150 mM phosphate buffer, pH 6, 150 mM NaCl, 4 °C. [b] Apparent dissociation constants were calculated by treating binding sites as independent of each other.

via gel electrophoresis. Agarose gels of the products are shown in Figure 3 and in Chapter 3 of the Supporting Information. For **III**, a broad band with lower mobility than that of the individual motifs was observed (Figure 3a). For **VII**, the supramolecular assemblies were so large that they did not migrate into the agarose gel at all (Figure 3b). Transmission electron microscopy showed large networks of material (Figure 3c), again confirming that hybridization via the sticky ends had occurred. Hybridization polymer **VIII** gave slower moving bands, the mobility of which depended on the initiator concentration employed (Figure S6, Supporting Information). Without initiator strand **VIII-3**, no oligomerization occurred. Low concentrations gave several slower moving bands, whereas increasing concentrations of the initiator gave the expected narrow length distribution of shorter assemblies.[32]

We then raised the concentration of strands to induce the formation of materials. At 0.1 mM concentration of either motif, the mixture of **I** and **II** gave a translucent hydrogel within 5 s of mixing/vortexing at 4 °C. This hydrogel was stable when allowed to warm to room temperature (Figure 4a). Control assembly **IV** also gave a hydrogel under these conditions (Figure S9, Supporting Information). The critical gelation constant (c_{gel}) of **III** was determined as approx. 60 μM through dilution, heating to 70 °C, cooling to 22 °C within 60 min, and inversion tests. This is an approximate value that assumes full folding and supramolecular assembly within the short time frame. At 0.1 mM concentration of **V** and **VI**, no solid or hydrogel formed under our experimental conditions, and **VII** was not pursued further. Linear hybridization polymer **VIII** gave a hydrogel at 0.3 mM concentration of the hairpins, 0.6 mM concentration of triplex-forming **VIII-4** and 1 μM initiator **VIII-3** (Figure 4c). However, the strand concentration required for macromolecular assembly was so high that polymer **VIII** was also not considered further for applications in flow cells.

Hydrogels **III** and **IV** were exposed to 50 μM solutions of FAD (ligand to binding site ratio of 1:1.1), and uptake was monitored by absorption at 450 nm. After 42 h at 4 °C the hydrogel of **III** had turned yellow (Figure 4b). Kinetics indicated that 60% of FAD was taken up within this time frame, so that the concentration in the supernatant dropped to 20 μM (Figure S10, Supporting Information). In contrast, control hydrogel **IV** took up just 5 μM FAD from the supernatant in 42 h.

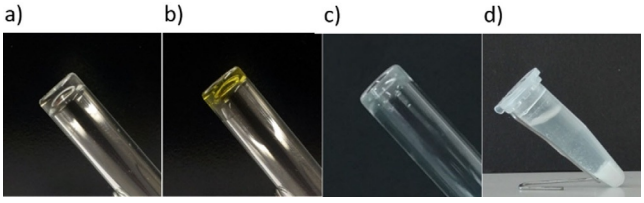

Figure 4. Photographs of samples of **III**, **VIII** and **X** at high concentrations. a) Hydrogel of **III** obtained at 0.1 mM concentration of **I** and **II**; b) same as a) after exposure to 50 μM FAD for 25 h at 4 °C and removal of the supernatant. c) hydrogel of **VIII**, obtained from 0.3 mM **VIII-1**, 0.3 mM **VIII-2**, 0.6 mM **VIII-4** and 1 μM initiator **VIII-3**) after 48 h at 22 °C. d) Material obtained upon treating 10 μM **X** with protamine (2 mg mL^{-1}; mass ratio of 1:2) after 10 min at 4 °C. Conditions: 10 mM phosphate buffer, 150 mM NaCl, 10 mM $MgCl_2$, pH 6.

While the uptake of FAD was significant, the properties of the hydrogels were not encouraging. No macroscopic flow through the gel could be induced, even when pressure was applied, and when release of the ligand was induced by warming to 37 °C, the entire hydrogel dissolved. We decided that this makes **III** unsuitable as active material for the flow cells envisioned for our apparatus.

We then turned to composite material **X**. Mixing a 10 μM solution of triplex **IX** with a solution of protamine at a ratio of 1:2 (w/w) resulted in the colorless precipitate shown in Figure 4d. A control experiment with FAD and protamine alone in the same buffer showed no precipitation (see Section 6 of the Supporting Information). The supernatant was then spiked with FAD solution at a molar ratio of 1:1 (FAD to binding sites). After 12 h at 4 °C, **X** had turned yellow, whereas material **XI** remained essentially colorless in the control assay.

This encouraged us to test **X** in a flow cell. Exploratory experiments with columns for automated DNA synthesis were successful, leading us to develop the experimental set-up shown in Figure 5a. It contains a silanized glass flow cell with a water jacket that allows for temperature control via a cuvette holder of a UV/Vis spectrophotometer with Peltier elements. Material **X** was placed between two membranes taken from DNA synthesizer columns to retain the active material. Silicone tubing connected the different parts of the set-up to allow for the flow of buffer solution with FAD through the cell. In a dif-

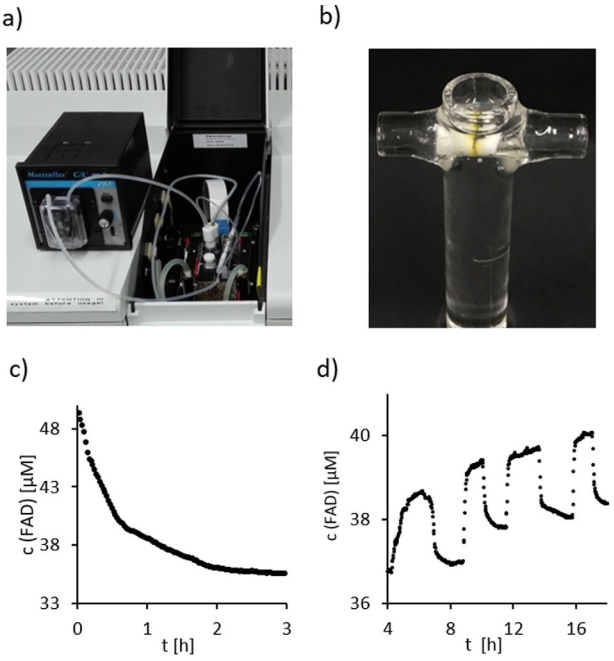

Figure 5. Loading and release of FAD from composite material **X** in a flow cell apparatus. a) Photograph of the experimental set-up, b) close-up view of the flow cell with FAD-loaded **X** between membranes c) Kinetics of uptake of FAD from the circulating solution, as monitored by UV/Vis absorption at 4 °C, and d) uptake at 4 °C and release at 37 °C of FAD through cyclic cooling and heating of the flow cell, measured in the same experimental set-up. Conditions: 25 nmol **X**, 125 nmol FAD (starting concentration 50 μM in 2.5 mL solution), buffer: 10 mM phosphate pH 6, containing 150 mM NaCl and 10 mM $MgCl_2$. Before loading, the ligand solution was pumped through the system for 1 h in order to equilibrate the system to 4 °C.

ferent compartment of the six-cell holder of the spectrophotometer was a flow cell for UV/Vis absorption measurements to monitor the FAD content of the solution circulated through the set-up by a peristaltic pump. Figure 5b shows a photograph of the flow-cell after loading with FAD. Additional photographs of the components of our flow set-up are provided in the Supporting Information (Figure S12).

Figure 5c shows the kinetics of loading **X** with FAD at 4 °C via uptake from the circulating solution. Within 3 h, 32% of the cofactor was taken up by **X**, employed with a stoichiometric number of binding sites, at a rate constant of 2.5 μM h^{-1} in the current set-up with 2.5 mL solution and 0.125 μmol FAD at 50 μM starting concentration, as determined by a single exponential fit. Little FAD (<9%) was bound by control material **XI** under the same conditions (Figure S13, Supporting Information).

The ability to bind cofactors was not limited to FAD as ligand. Binding experiments with ATP gave 25% uptake from the 50 μM solution of this triphosphate by **X** within 4 h. Again, the uptake was selective, with 2% uptake by control material **XI** (Figure S13, Supporting Information).

Figure 5d shows the result of four loading and discharging cycles in the same set-up. Loading was at 4 °C, and the release of FAD was induced by setting the temperature of the cell holder housing the cells of the system to 37 °C. The results show that the flavin-containing cofactor is bound reversibly in temperature-controlled fashion with little loss of capacity. Further optimization of the system is expected to reduce the drift in the baseline.

Finally, we tested whether the ligand released from the flow cell can be used to drive a biochemical reaction. For this, we chose a luciferase assay with ATP as cofactor. Figure 6a shows the experimental set-up in cartoon format, and Figure 6b and 6c show photographs of the glass vial in which the biochemical assay solution had been placed under ambient light and in the dark, where the bioluminescence was readily observed. The results of the proof-of-principle experiment indicated that the flow cell does indeed release the cofactor at biochemically relevant levels in temperature-controlled fashion. This demonstrated that a replaceable "biochemical battery" can be constructed to drive energy-consuming processes without electricity or combustion of any kind.

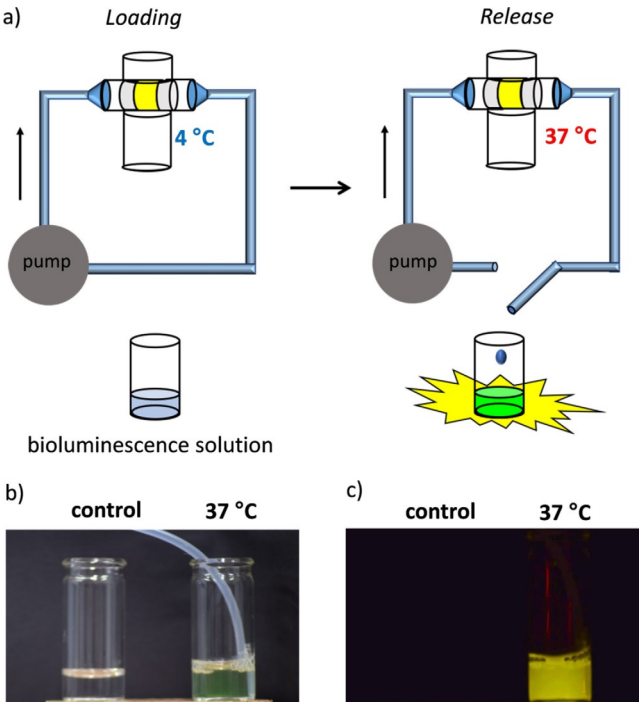

Figure 6. Bioluminescence reaction fed by ATP released from a flow cell containing **X** loaded with ATP. a) Cartoon of the experimental set-up during loading and release phase, respectively. b) Photographs of glass vials with luciferase assay solution in ambient light. The vial on the right is being fed with solution from the flow set-up with the flow cell at 37 °C; c) same as b) with photograph taken in the dark. Conditions: 25 nmol **X**, previously loaded using 2.5 mL of a 50 μM solution of ATP in 10 mM phosphate buffer, pH 6, 150 mM NaCl, 10 mM $MgCl_2$. After 3.5 h of loading at 4 °C, the ligand solution had been removed, and the flow cell was washed with ATP-free phosphate buffer (10 mM, pH 6, 150 mM NaCl, 10 mM $MgCl_2$) at 4 °C for 5 min. Release was induced by warming and pumping luciferase assay buffer through the set-up with the release solution running into the glass vial containing a solution of 2 mg luciferase/luciferin in 1 mL luciferase buffer.

Conclusions

A flow cell containing a composite biomaterial based on DNA and protamine was developed. The flow cell acts as a "biochemical battery" in that it takes up adenine-containing cofactors from aqueous buffer in the cold and releases the cofactor upon warming to body temperature. The active material of the flow cell is biodegradable and survives several cycles of loading and release. Experiments with luciferase indicate that the battery-like flow cell can be used in designed bioprocesses, such as our proof-of-principle application that produces light. Our approach for generating an active material from soluble DNA binding motifs may become useful for other DNA assemblies, opening the door to a novel type of biotechnology that employs portable and rechargeable flow cells to drive biochemical of biological process.

Experimental Section

General

Unmodified oligonucleotides were purchased from Biomers (Ulm, Germany) or IDT-DNA (Leuven, Belgium) in HPLC-purified form and were used without modification. Strand **IX-1** was prepared as described in the Supporting Information, using a known C3 linker phosphoramidite.[19] Flavin adenine dinucleotide (FAD) was from Alfa Aesar (Karlsruhe, Germany); ATP and protamine from Salmon (grade IV, histone-free) were from Sigma–Aldrich (Taufkirchen, Germany). The flow apparatus contained a MasterFlex C L^{-1} peristaltic pump, model No. 77122-14, (Cole Palmer, Vernon Hills, Illinois), a QS 10 flow cuvette (Hellma Analytics, Müllheim, Germany), a Lamda 25 spectrophotometer (PerkinElmer, Rodgau, Germany) with Peltier-controlled six-cell holder, and silicon tubing with 1 mm inner diameter (Carl Roth, Karlsruhe, Germany). The membranes (5 mm diameter) used in the flow cell were from synthesis columns for automated DNA-synthesis from Sigma–Aldrich (Taufkirchen,

Germany). The luciferase luminescence assay used an ATP Biomass Kit HS (BioThema, Handen, Sweden).

Supramolecular assemblies

Hydrogel of Y-motifs: Stock solutions of Y-motifs **I** and **II** in phosphate buffer (10 mM), pH 6 containing NaCl (150 mM) and $MgCl_2$ (10 mM) were mixed at 4 °C to give a 60 μM concentration of each motif, followed by vortexing for 5 s. The resulting hydrogel was then allowed to warm to 22 °C.

Soluble assemblies of square motifs: Solutions of square motifs **V** (4 μM) and **VI** (4 μM) in aqueous buffer (250 μL, 10 mM phosphate, pH 6, 150 mM NaCl, 10 mM $MgCl_2$) were mixed at 4 °C. Annealing in a thermocycler used a linear temperature gradient from 85 ° C to 4 °C in 72 h.

Hybridization polymer: Stock solution of oligonucleotides were combined to give the desired final concentrations of **VIII-1** (300 μM), **VIII-2** (300 μM), **VIII-3** (1 μM) and **VIII-4** (600 μM) in phosphate buffer (10 mM, pH 6) containing NaCl (150 mM) and $MgCl_2$ (10 mM). The hybridization led to a DNA-hydrogel within 48 h at 22 °C.

Composite material X: Material formation was induced by mixing a protamine solution (2 mg mL^{-1}) containing NaCl (150 mM), phosphate buffer (10 mM, pH 6) and pre-annealed motif **IX** or the control motif (10 μM) in phosphate buffer (10 mM, pH 6) containing NaCl (150 mM) at a ratio of 2:1 in Protein LoBind Tubes (Eppendorf AG, Hamburg, Germany) at 4 °C. The solution turned cloudy immediately. Vortexing for 5 s promoted the formation of a material that started to precipitate. The suspension was kept at 4 °C for 30 min in order to complete precipitation. The supernatant was decanted, and the material was aspirated into the flow cell using the peristaltic pump.

Binding and release of cofactors with flow cell

The flow system consists of a glass cell, a degassing vessel meant to shed bubbles and acting as a reservoir, a peristaltic pump and a flow cuvette. All parts were connected by silicon tubes (1 mm inner diameter). The glass cell, the degassing vessel, and the flow cuvette were placed into slots of a Peltier-controlled six-cell holder of the spectrophotometer. The amount of ligand solution was calculated to give a ratio of binding sites to ligand of 1:1. Before use, the ligand solution of FAD or ATP (50 μM, 2.5 mL) in phosphate buffer (10 mM, pH 6, 150 mM NaCl, 10 mM $MgCl_2$) was pumped through the set-up for 1 h at 0.7 mL min^{-1} to equilibrate at 4 °C. Then **X** or **XI** (25 nmol motifs) was placed between the two porous membranes of the flow cell. Using the flow cuvette, the absorption of the circulating ligand solution was monitored over time. Loading was at 4 °C, release was at 37 °C.

Bioluminescence assay

An aqueous solution of ATP (50 μM, 2.5 mL) in phosphate buffer (10 mM, pH 6, 150 mM NaCl, 10 mM $MgCl_2$) was pumped through the flow set-up for 1 h at 0.7 mL min^{-1} and 4 °C. A flow cell containing **X** (25 nmol) obtained from **IX** (25 nmol, 10 μM) and precipitated with protamine as described above was placed in the flow set-up, followed by pumping at 4 °C for 3.5 h. The circulating solution was removed and the system was washed at 4 °C with phosphate buffer (10 mM, pH 6, 150 mM NaCl, 10 mM $MgCl_2$) for 5 min to remove excess ATP. Release of ATP occurred at 37 °C. For this, Diluent Buffer (2.5 mL, ATP Biomass Kit HS) was pumped through the flow system at 37 °C for 2 min without flow cell, then the flow was directed through the flow cell, and allowed to drip (0.7 mL min^{-1}) into the glass vial containing the solution of luciferase and luciferin (2 mg in 1 mL Diluent Buffer). Photographs were taken with a Nikon DSLR D3300 camera with an exposure time of 15 s.

Acknowledgements

The authors thank Sven Vollmer for sharing results, and Helmut Griesser for a review of parts of the manuscript. Financial support by Stiftung Energieforschung Baden-Württemberg (SEF, grant No. A 308) is gratefully acknowledged.

Conflict of interest

The authors declare no conflict of interest.

Keywords: cofactors · DNA · flow cell · nanostructures · triplexes

[1] N. C. Seeman, *Nature* **2003**, *421*, 427 – 431.
[2] P. W. K. Rothemund, *Nature* **2006**, *440*, 297 – 302.
[3] B. Wei, M. Dai, P. Yin, *Nature* **2012**, *485*, 623 – 626.
[4] a) F. C. Simmel, *Angew. Chem. Int. Ed.* **2008**, *47*, 5884 – 5887; *Angew. Chem.* **2008**, *120*, 5968 – 5971; b) B. Saccà, C. M. Niemeyer, *Angew. Chem. Int. Ed.* **2012**, *51*, 58 – 66; *Angew. Chem.* **2012**, *124*, 60 – 69; c) M. R. Jones, N. C. Seeman, C. A. Mirkin, *Science* **2015**, *347*, 1260901.
[5] K. E. Dunn, F. Dannenberg, T. E. Ouldridge, M. Kwiatkowska, A. J. Turberfield, J. Bath, *Nature* **2015**, *525*, 82 – 86.
[6] a) K. F. Wagenbauer, C. Sigl, H. Dietz, *Nature* **2017**, *552*, 78 – 83; b) N. Liu, T. Liedl, *Chem. Rev.* **2018**, *118*, 3032 – 3053.
[7] H. Dietz, S. M. Douglas, W. M. Shih, *Science* **2009**, *325*, 725 – 730.
[8] E. S. Andersen, M. Dong, M. M. Nielsen, K. Jahn, R. Subramani, W. Mamdouh, M. M. Golas, B. Sander, H. Stark, C. L. P. Oliveira, J. S. Pedersen, V. Birkedal, F. Besenbacher, K. V. Gothelf, J. Kjems, *Nature* **2009**, *459*, 73 – 76.
[9] N. V. Voigt, T. Tørring, A. Rotaru, M. F. Jacobsen, J. B. Ravnsbæk, R. Subramani, W. Mamdouh, J. Kjems, A. Mokhir, F. Besenbacher, K. V. Gothelf, *Nat. Nanotechnol.* **2010**, *5*, 200 – 203.
[10] I. J. Tetlow, *Seed Sci. Res.* **2011**, *21*, 5 – 32.
[11] H. C. Kim, D. M. Kim, *J. Biosci. Bioeng.* **2009**, *108*, 1 – 4.
[12] J. Kim, C. B. Park, *Curr. Opin. Chem. Biol.* **2019**, *49*, 122 – 129.
[13] I. Zachos, C. Nowak, V. Sieber, *Curr. Opin. Chem. Biol.* **2019**, *49*, 59 – 66.
[14] M. Sassanfar, J. W. Szostak, *Nature* **1993**, *364*, 550 – 553.
[15] E. I. Campos, D. Reinberg, *Annu. Rev. Genet.* **2009**, *43*, 559 – 599.
[16] C. Kröner, M. Röthlingshöfer, C. Richert, *J. Org. Chem.* **2011**, *76*, 2933 – 2936.
[17] M. Patel, A. Dutta, H. A. Huang, *Anal. Bioanal. Chem.* **2011**, *400*, 3035 – 3040.
[18] S. Vollmer, C. Richert, *Org. Biomol. Chem.* **2015**, *13*, 5734 – 5742.
[19] S. Vollmer, C. Richert, *Chem. Eur. J.* **2015**, *21*, 18613 – 18622.
[20] C. Kröner, M. Thunemann, S. Vollmer, M. Kinzer, R. Feil, C. Richert, *Angew. Chem. Int. Ed.* **2014**, *53*, 9198 – 9202; *Angew. Chem.* **2014**, *126*, 9352 – 9356.
[21] C. Kröner, A. Göckel, W. Liu, C. Richert, *Chem. Eur. J.* **2013**, *19*, 15879 – 15887.
[22] J. Zheng, J. J. Birktoft, Y. Chen, T. Wang, R. Sha, R. E. Constantinou, S. L. Ginell, C. Mao, N. C. Seeman, *Nature* **2009**, *461*, 74 – 77.
[23] P. J. Paukstelis, *J. Am. Chem. Soc.* **2006**, *128*, 6794 – 6795.
[24] M. Meng, C. Ahlborn, M. Bauer, O. Plietzsch, S. A. Soomro, A. Singh, T. Muller, W. Wenzel, S. Bräse, C. Richert, *ChemBioChem* **2009**, *10*, 1335 – 1339.
[25] A. Schwenger, N. Birchall, C. Richert, *Eur. J. Org. Chem.* **2017**, 5852 – 5864.
[26] H. Griesser, A. Schwenger, C. Richert, *ChemMedChem* **2017**, *12*, 1759 – 1767.

[27] A. Schwenger, T. P. Jurkowski, C. Richert, *ChemBioChem* **2018**, *19*, 1523 – 1530.
[28] P. L. Husler, H. H. Klump, *Arch. Biochem. Biophys.* **1995**, *322*, 149 – 166.
[29] D. A. Rusling, A. R. Chandrasekaran, Y. P. Ohayon, T. Brown, K. R. Fox, R. Sha, C. Mao, N. C. Seeman, *Angew. Chem. Int. Ed.* **2014**, *53*, 3979 – 3982; *Angew. Chem.* **2014**, *126*, 4060 – 4063.
[30] C. R. Simmons, F. Zhang, J. J. Birktoft, X. Qi, D. Han, Y. Liu, R. Sha, H. O. Abdallah, C. Hernandez, Y. P. Ohayon, N. C. Seeman, H. Yan, *J. Am. Chem. Soc.* **2016**, *138*, 10047 – 10054.
[31] Q. Zhang, Y. Wang, X. Meng, R. Dhar, H. Huang, *Anal. Chem.* **2013**, *85*, 201 – 207.
[32] R. M. Dirks, N. A. Pierce, *Proc. Natl. Acad. Sci. USA* **2004**, *101*, 15275 – 15278.
[33] D. Lochmanna, J. Weyermanna, C. Georgensa, R. Prasslb, A. Zimmer, *Eur. J. Pharm. Biopharm.* **2005**, *59*, 419 – 429.

Manuscript received: August 8, 2019
Revised manuscript received: September 3, 2019
Accepted manuscript online: September 4, 2019
Version of record online: October 22, 2019

